

Original citation:

Zhang, Guohui, Walker, Marc and Unwin, Patrick R.. (2016) Low-voltage voltammetric electrowetting of graphite surfaces by ion intercalation/deintercalation. *Langmuir*, 32 (30). pp. 7476-7484.

Permanent WRAP URL:

<http://wrap.warwick.ac.uk/81638>

Copyright and reuse:

The Warwick Research Archive Portal (WRAP) makes this work by researchers of the University of Warwick available open access under the following conditions. Copyright © and all moral rights to the version of the paper presented here belong to the individual author(s) and/or other copyright owners. To the extent reasonable and practicable the material made available in WRAP has been checked for eligibility before being made available.

Copies of full items can be used for personal research or study, educational, or not-for profit purposes without prior permission or charge. Provided that the authors, title and full bibliographic details are credited, a hyperlink and/or URL is given for the original metadata page and the content is not changed in any way.

Publisher's statement:

"This document is the Accepted Manuscript version of a Published Work that appeared in final form in *Langmuir*. copyright © American Chemical Society after peer review and technical editing by the publisher.

To access the final edited and published work

<http://pubs.acs.org/page/policy/articlesonrequest/index.html> ."

A note on versions:

The version presented here may differ from the published version or, version of record, if you wish to cite this item you are advised to consult the publisher's version. Please see the 'permanent WRAP URL above for details on accessing the published version and note that access may require a subscription.

For more information, please contact the WRAP Team at: wrap@warwick.ac.uk

Low-voltage Voltammetric Electrowetting of Graphite Surfaces by Ion Intercalation/De-intercalation

Guohui Zhang,[†] Marc Walker[‡] and Patrick. R. Unwin^{*†}

[†] Department of Chemistry, University of Warwick, Coventry CV4 7AL, United Kingdom.

[‡] Department of Physics, University of Warwick, Coventry CV4 7AL, United Kingdom.

Abstract

We demonstrate low-voltage electrowetting at the surface of freshly cleaved highly oriented pyrolytic graphite (HOPG). Using cyclic voltammetry (CV), electrowetting of a droplet of sodium perchlorate solution is observed at moderately positive potentials on high-quality (low step edge coverage) HOPG, leading to significant changes in contact angle and relative contact diameter that is comparable to the widely studied electrowetting on dielectric (EWOD) system, but over a much lower voltage range. The electrowetting behavior is found to be reasonably fast, reversible and repeatable for at least 20 cyclic scans (maximum tested). In contrast to classical electrowetting, e.g. EWOD, the electrowetting of the droplet on HOPG occurs with the intercalation/de-intercalation of anions between the graphene layers of graphite, driven by the applied potential, observed in the CV response, and detected by X-ray photoelectron spectroscopy. The electrowetting behavior is strongly influenced by those factors that affect the extent of the intercalation/de-intercalation of ions on graphite, such as scan rate, potential polarity, quality of the HOPG substrate (step edge and step height), and type of anion in the solution. In addition to perchlorate, sulfate salts also promote electrowetting, but some other salts do not. Our findings suggest a new mechanism for electrowetting based on ion intercalation and the results are of importance to fundamental

electrochemistry, as well as diversifying the means by which electrowetting can be controlled and applied.

Introduction

The wetting of substrates by liquid droplets has long aroused great interest in the scientific community, driven by a number of applications, such as surface coatings,¹ oil/water separation² and (nano)pattern fabrication.³ Electrowetting describes the influence of an electric field on wetting, and has been the subject of many fundamental studies.^{4, 5, 6, 7} Applications include electronic displays,⁸ optical lenses⁹ and lab-on-a-chip systems.¹⁰ Electrowetting can be used to electronically control small amounts of liquid, without the mechanical movement of components, which is of paramount importance in microfluidic devices,^{4, 11} and considerable attention derives from this particular application.

Hitherto, electrowetting has been achieved most readily with an electrowetting-on-dielectric (EWOD) format.^{12, 13} In this situation, a liquid droplet is placed on a dielectric-layer coated electrode, with the electrode and droplet essentially acting as the two plates of a capacitor. Through the application of an external potential difference between the substrate electrode and an electrode in the droplet, the electrode/dielectric and droplet/dielectric interfaces can be charged, producing a change of the contact angle (CA) of the droplet.^{4, 13} An advantage of this configuration is that complications from the electrolysis of the electrolyte are avoided.

EWOD can produce quite large changes in CA, but because of the dielectric film very high voltages (20~300 V) usually have to be applied.^{5, 12, 14, 15} The dynamics of electrowetting are rapid in this format, making it difficult to monitor the wetting dynamics.¹⁶ Conductive surfaces, such as steel¹⁷ and graphene/carbon nanotube films,¹⁸ are being thus explored to lower the voltage and increase the timescale of electrowetting. However, the electrowetting is very slow and not readily reversible.¹⁷

In this work, we demonstrate an entirely new mechanism of electrowetting of a substrate by a droplet, promoted by ion intercalation/de-intercalation into highly oriented pyrolytic graphite

(HOPG). The process is promoted by cyclic voltammetry (CV) conditions over a low potential range (0~+2 V vs Ag/AgCl quasi-reference electrode), and is highly reversible and fairly fast. HOPG is characterized by an easy surface preparation by mechanical cleavage, and has a well-defined surface structure (i.e. extensive basal plane areas and step edges).¹⁹ It is composed of stacked graphene layers, which serve as host sites for ion intercalation and ion intercalation is considered to be important for the production of graphene flakes via exfoliation.²⁰ It has been reported that compounds containing ClO_4^- , SO_4^{2-} and NO_3^- ions are graphite intercalators that can expand the spacing between graphitic layers (0.335 nm) at positive potentials, due to their slightly larger ionic size and negative charge. However, there is no intercalation of PO_4^{3-} ions into graphite.^{21, 22, 23} In the studies herein, we control the potential to avoid exfoliation and explore the factors that promote electrowetting and its associated timescale. Our work provides intriguing insights into the effect of step edge density on electrowetting, with the highest quality HOPG samples that have low step edge density (but monolayer steps) leading to more facile ion intercalation/de-intercalation and thus extensive electrowetting. In contrast, HOPG samples with much higher step edge densities, but with multilayer steps, show much less significant electrowetting. The results we present are thus important not only for characterizing this new mechanism of electrowetting, but also for providing significant new information on ion intercalation into carbon electrodes, which has many technical applications (e.g. in battery electrodes).²⁴

Experimental section

Materials and Chemicals

Sodium perchlorate (NaClO_4 , $\geq 98\%$), sodium phosphate tribasic dodecahydrate ($\text{Na}_3\text{PO}_4 \cdot 12\text{H}_2\text{O}$, $\geq 98\%$), sodium sulphate (Na_2SO_4 , $\geq 99\%$), fluorescein sodium salt ($\text{C}_{20}\text{H}_{10}\text{O}_5\text{Na}_2$) and phosphoric acid (H_3PO_4 , $\geq 85\%$) were purchased from Sigma-Aldrich. All the solutions were

freshly prepared using water purified with a Millipore Milli-Q system (resistivity 18.2 M Ω cm at 25 °C). The solution of Na₃PO₄ was adjusted to a pH ~7 with the aid of H₃PO₄ before use, under which conditions the predominant forms of anion in the solution are HPO₄²⁻ and H₂PO₄⁻.²⁵ A high quality, but ungraded HOPG sample was kindly provided by Prof. Richard L. McCreery (University of Alberta, Canada), originating from Dr. Arthur Moore, Union Carbide (now GE Advanced Ceramics) and termed AM grade HOPG henceforth (as defined in previous papers from our group^{19, 26, 27, 28, 29}). Fresh pieces were cleaved immediately prior to use that had a thickness of about 0.8 mm. SPI-3 grade HOPG was obtained from SPI Supplies (Aztech Trading, UK), and the piece used had a thickness of 1 mm.

For the electrowetting measurements, we used a two-electrode configuration, in which the HOPG sample was employed as the working electrode (WE), and an AgCl-coated Ag wire served as a combined counter/reference electrode (CE/RE). The experimental setup is illustrated in Figure 1a. Before each measurement, HOPG samples were cleaved with Scotch tape, to generate a fresh surface. The two grades of HOPG used show significantly different step edge coverage, as seen from the typical AFM images in Figure 1b and reported previously.^{19, 27, 28, 30, 31} After cleavage of the HOPG samples, a 5 μ L droplet of the solution of interest was gently placed atop the surface in a quick motion, followed by the assembly of the Ag/AgCl wire into the droplet, as described elsewhere.^{28, 32} CV was then immediately carried out with a custom-made potentiostat, with the potential window and scan rate controlled by the LabVIEW interface of an FPGA card (National Instruments). The data acquisition rate was typically 389 data points per second, each point being the average of 256 samples. This produced a potential resolution of 2.6 mV per data point for the scan rate of 1 V s⁻¹ and finer potential resolution at slower scan rates.

Optical images of droplet electrowetting on the HOPG surface during CV scans were recorded simultaneously by using a camera (PixeLINK PL-B782U, equipped with a 2 \times

magnification lens) with 1920×1080 pixels, at a frame rate of 12.5 fps, being controlled by the LabVIEW program so that images could be correlated precisely with CV data. The resulting images of droplet electrowetting under CV conditions were analyzed with the SPIP (Scanning Probe Image Processor) software package. The CA for the droplet at a particular potential was measured three times at the contact line and the average value was adopted. The relative contact diameter (RCD) of the droplet was defined as the ratio of contact diameter of droplet at a particular applied voltage to that of the pristine droplet (at 0 V bias). All experiments were performed at room temperature (20 °C).

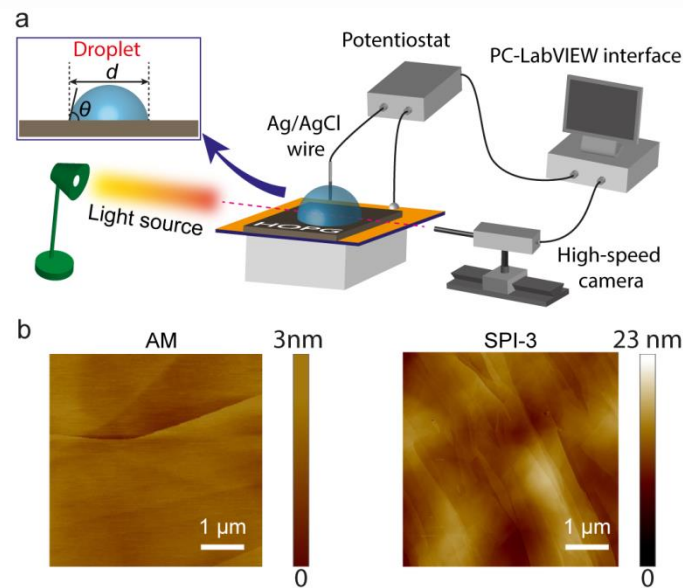


Figure 1. (a) Schematic illustration of the experimental setup of droplet electrowetting measurements on HOPG (not to scale), with the contact angle (θ) and contact diameter (d) shown in the upper left inset. (b) $5 \times 5 \mu\text{m}$ tapping-mode AFM images of AM and SPI-3 grade HOPG. Note the difference in the height scale.

X-ray photoelectron spectroscopy (XPS) data were collected using an Omicron Multiprobe at the University of Warwick Photoemission Facility. Two samples were prepared with a droplet of 1mM NaClO₄. One was an electrochemically-treated sample that was subjected to 30 repetitive CVs from 0 V to +2 V at a scan rate of 1 V s⁻¹, before being held at +1.5 V (on the reverse scan) for 30 s. With the substrate held at this potential, the electrical contact was then disconnected and the droplet was removed with a short blast from an argon gas gun. The second sample was a control, where there was no electrochemistry, but the droplet was on the AM HOPG surface for the same time as the one subjected to electrochemistry, before removing the droplet in the same fashion. The HOPG samples were mounted on Omicron sample plates using electrically-conductive carbon tape and immediately loaded into the fast-entry chamber. Once a pressure of less than 1×10^{-7} mbar had been achieved, the samples were transferred to a 12-stage storage carousel, located between the preparation and main analysis chambers, for storage at a pressure of less than 2×10^{-10} mbar. XPS measurements were conducted in the main analysis chamber (base pressure 2×10^{-11} mbar), with the sample being illuminated using an XM1000 monochromatic Al $\kappa\alpha$ x-ray source (Omicron Nanotechnology). The measurements were conducted at room temperature and at a take-off angle of 90° with respect to the sample surface. The photoelectrons were detected using a Sphera electron analyzer (Omicron Nanotechnology), with the core level spectra recorded using a pass energy of 20 eV (resolution approx. 0.63 eV). The data were analyzed using the CasaXPS package, using Shirley backgrounds, mixed Gaussian-Lorentzian (Voigt) lineshapes and asymmetry parameters, where appropriate. All binding energies were calibrated using the Fermi edge of a polycrystalline Ag sample, measured immediately prior to commencing the measurements. Compositional accuracy was ensured by calibrating the transmission function of the spectrometer using a variety of clean metal foils.

Results and Discussion

In this study, we applied a set of positive and negative potential windows to the droplet cell (5 μL), by scanning the substrate potential from 0 V (vs Ag/AgCl wire; to which all potentials are referred) up to a defined positive or negative limit. Note that the Ag/AgCl wire has a reasonably stable potential³³ (ca. +140 mV vs saturated calomel electrode, as measured in this study). In both directions, the potential limits were gradually expanded to a maximum of ± 2 V, enabling the wettability of HOPG to be explored in a variety of potential ranges. Compared to the droplet size, the Ag/AgCl electrode, which was produced on an Ag wire that was polished to generate a sharp end before the deposition of AgCl, had negligible effect on the shape and geometry of the droplet resting on the surface of HOPG. Meanwhile, the effect of gravity on the droplet can be ignored, as the droplet size (typically 1.4 mm radius) is smaller than the capillary length, expressed as $(\gamma_{LV}/\rho g)^{1/2}$, where γ_{LV} is the liquid-solid surface tension (typically 72.8 dyn cm^{-1}), with ρ , g respectively representing the density of the aqueous solution (~ 1 g cm^{-3}) and the gravitational acceleration (9.8 m s^{-2}).^{12, 34} Therefore, any change in the CA and RCD of the droplets during CV measurements can be ascribed to the applied voltage (*vide infra*).

Voltage effect on electrowetting

A CA of $\sim 51^\circ$ was observed for aqueous (1 mM NaClO_4) droplets on freshly cleaved AM HOPG surfaces with no applied electric field. This result is in line with other studies that have shown graphite surfaces to be mildly hydrophilic with a contact angle of about 50° ,^{35, 36, 37} Although higher aqueous contact angle values have been reported in the literature,^{38, 39, 40} variations are expected depending on the sample quality, measurement environment (including surface contamination which increases the contact angle) and droplet size.^{35, 36, 41} Given the short timescale (< 5 s) on which the droplet was deposited after cleavage of surface,

the value we report can be taken as the intrinsic CA of 1 mM NaClO₄ at AM HOPG, and is in line with theoretical predictions.³⁶

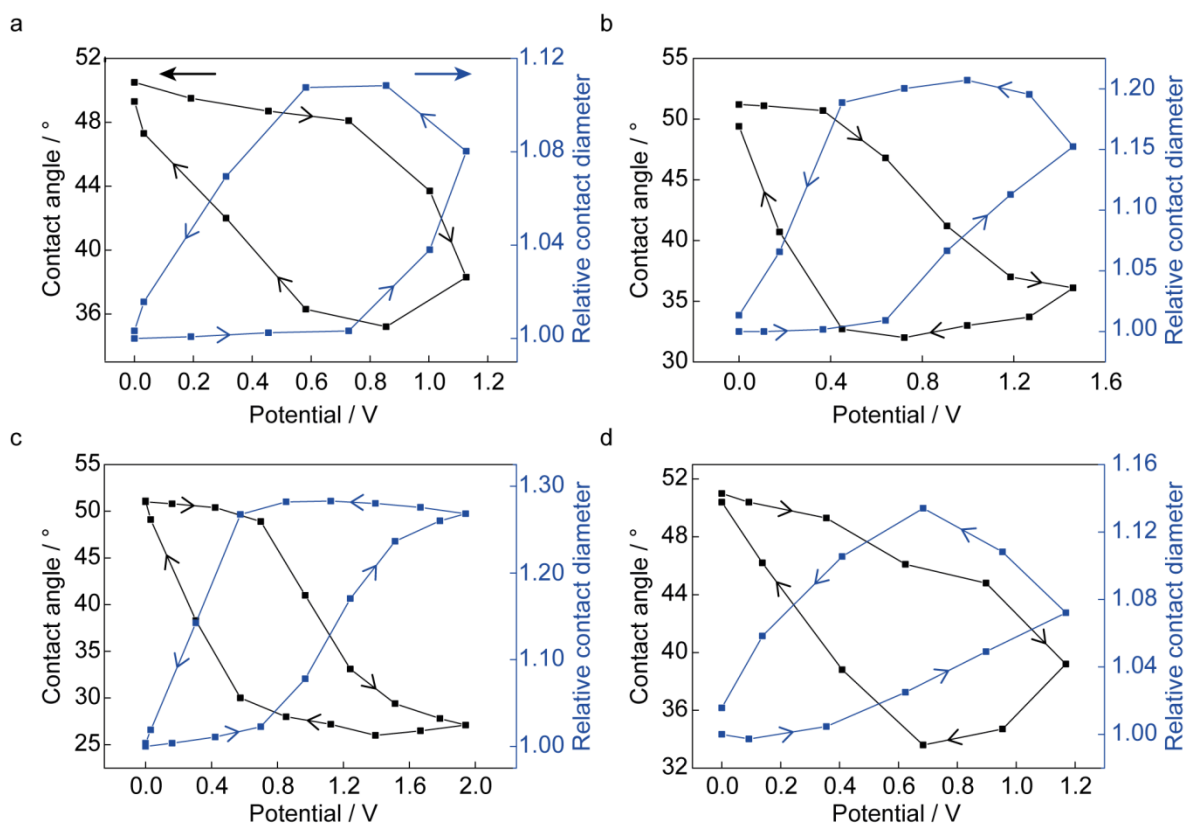


Figure 2. Contact angle and relative contact diameter for a droplet of 1 mM NaClO₄ solution at the surface of AM HOPG, during cyclic voltammograms recorded in the potential range of (a) 0 to +1.2 V, (b) 0 to +1.5 V, (c) 0 to +2 V and finally (d) 0 to +1.2V after the scan from 0 to +2 V, at a scan rate of 1 V s⁻¹ in each case. Note that the difference in the scale of the contact angles and the directions indicated by arrows in each plot.

When the applied potential was scanned positively, the droplet was found to electrowet the substrate as evidenced by the spreading (advancing) and retraction (receding) of the droplet,

as manifest in the changes in CA and RCD (Figure 2). In the potential range of 0~+1.2 V (Figure 2a), the droplet spread with increasing positive potential, with RCD increasing by ca. 11 % at +1.13 V, while the CA was reduced from 51° to 38°. Note that similar behavior was observed with an electrolyte concentration of 0.1 M (data reported in Supporting Information, section S1). Interestingly, there is a clear hysteresis of both the CA and RCD between the outgoing and return scans which, in part, is due to the wetting lagging the change of potential at this scan rate. In fact, as a consequence, the maxima of the CA and RCD are seen on the reverse scan. Thus, for electrowetting of AM HOPG by the droplet in Figure 2a, a minimum CA of 35° and a maximum RCD of 1.11 are seen at +0.86 V on the reverse scan. As the potential was returned to zero, the droplet retracted back towards its original shape, increasing the CA to ~50° at 0 V, which was slightly lower than at the beginning of the scan, with a slightly higher RCD (Figure 2a).

When the upper potential limit of the CV was increased to +1.5 V on the same sample (Figure 2b), there was a decrease of the CA by 15° (from 51° to 36°) and an increase of 15 % in RCD. A minimum CA of 32° and a maximum RCD of 1.2 were observing at +0.72 V on the reverse scan. In the case of +2 V being the positive limit (Figure 2c), the CA dropped dramatically by 25°, from 51° with no potential applied to 26° at +1.4 V on the reverse scan and meanwhile the RCD was enlarged by 28%. The wettability of AM HOPG after the scan between 0 V and +2 V was revisited by performing a CV in the potential range of 0~+1.2 V. It was found that the electrowetting behavior of the droplet was enhanced slightly (compare Figure 2a to Figure 2d), suggesting some change in the surface properties, which we consider further below.

The optical images in Figure 3 (extracted from a typical movie recorded during a CV measurement; see Supporting Information, the movie 'Electrowetting of AM HOPG')

illustrate the significant droplet electrowetting on AM HOPG during the CV carried out from 0 to +2 V. Good repeatability of this behavior was observed for at least 20 repetitive cycles (see Supporting Information, section S2), although, there is a change of the electrowetting potential region with the number of scans from 1 to 5 (to more cathodic values), with the electrowetting potential window and behavior remaining fairly consistent thereafter.



Figure 3. Snapshot optical images for a droplet of 1 mM NaClO₄ solution on AM HOPG during cyclic voltammetry, with the potential swept in the range of 0~+2 V, recorded with the potential increased from (a) 0 V, to (b) +1.4 V and (c) decreased back to 0 V (vs Ag/AgCl), with the corresponding contact angle values indicated. The scan rate was 1 V s⁻¹.

Our experimental method allowed the electrochemical responses to be recorded simultaneously during voltammetric electrowetting. The data for a 1 mM NaClO₄ droplet on AM HOPG are shown in Figure 4 (also see Supporting Information, section S3). For the anodic scan to a potential limit of +1.2 V, a small oxidation peak at +0.85 V was detected on the outgoing scan, with a hint of reduction at ca. +0.2 V on the reverse (Figure 4a). When the upper potential limit was increased to +1.4 V for the same HOPG surface, the oxidation feature was again seen, with a clearer reduction peak at +0.3 V (Figure 4b). With the positive potential limit increased further to +1.6 V, the anodic peak was seen even more clearly, followed by an anodic process, likely due to the onset of water oxidation. The corresponding reduction peak on the reverse scan became more pronounced and shifted positively to +0.34

V (Figure 4c), +0.37 V (Figure 4d) and +0.4 V (Figure 4e). After the set of voltammetric scans in Figures 4a-e, a voltammogram over the potential range of 0~+1.2 V was recorded, and the reduction peak was still noticeable (at +0.31 V vs Ag/AgCl) on the cyclic voltammogram (Figure 4f) and much more prominent than the initial scan over the same range (Figure 4a). The development of the reduction peak with the increase in the upper positive potential limit and number of potential scans (also see additional data in Supporting Information, section S3) correlates with the enhanced electrowetting behavior observed for the droplet on AM HOPG (*vide supra*, Figure 2).

The oxidation-reduction process observed as the pair of peaks identified could be due to the intercalation/de-intercalation of anions,⁴² or related to surface quinone-hydroquinone redox conversion (or other surface oxidation/reduction processes).⁴³ As we demonstrate below, the former process is most likely and is responsible for the electrowetting seen for the aqueous droplet.

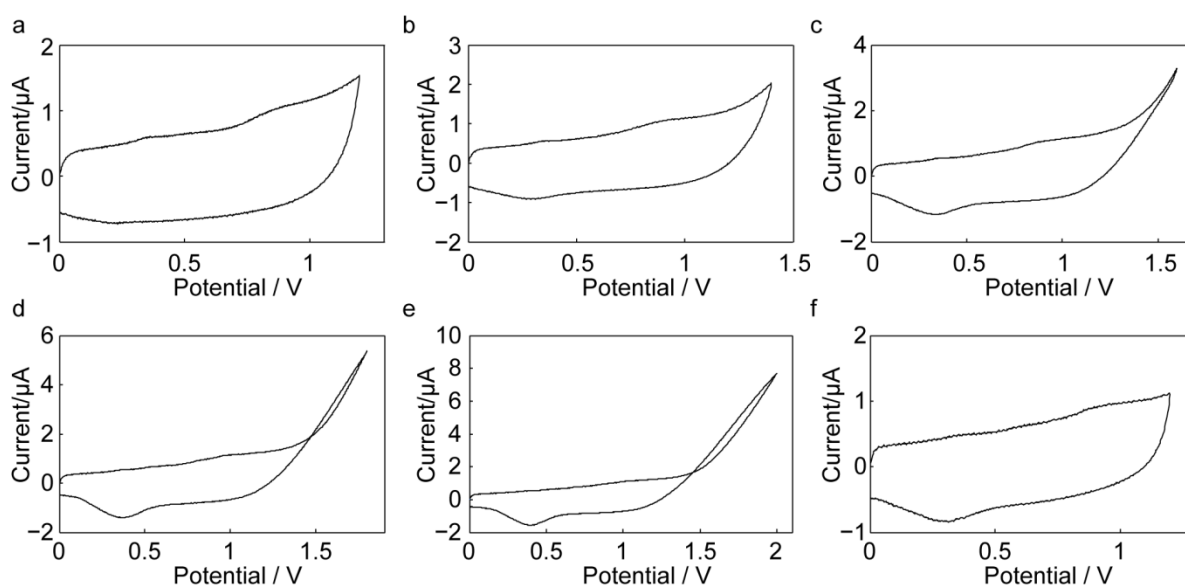


Figure 4. Cyclic voltammograms for a droplet of 1 mM NaClO₄ on AM HOPG with applied voltage in the range of (a) 0~+1.2 V, (b) 0~+1.4 V, (c) 0~+1.6 V, (d) 0~+1.8 V, (e) 0~+2 V and (f) 0~+1.2 V after the CV swept between 0 and +2 V. Scan rate: 1 V s⁻¹.

On the forward scan of the CV (oxidation), ClO_4^- ions from the aqueous droplet can be driven into graphite through exposed step edges, overcoming the van de Waals forces between the graphene sheets.^{44, 45} This intercalation reaction is defined in eqn. (1), and correlates to the small oxidation peak at $\sim +0.85$ V and beyond:



It has also been reported that side reactions, such as carbon oxidation and water splitting, occur at anodic potentials and might be responsible for the anodic currents we see at more positive potentials.^{22, 42} However, the surface oxidation process is slow and would not be expected to change the surface significantly and promote electrowetting, as we show with further measurements below.⁴⁶ Rather extreme conditions of potential, time and electrolyte are needed to produce significant changes to the graphite surface, such as exfoliation,^{47, 48} and these processes can be ruled out.

On the reverse scan of the CV (reduction), the de-intercalation of ClO_4^- from the graphite leads to the reduction peak observed on the CV (Figure 4 and Figure S3). As the upper potential limit was increased with further scans, it can be seen that intercalation/de-intercalation becomes more favored, i.e. repetitive cycling leads to a break-in of the surface towards intercalation/de-intercalation. We examined AM HOPG by atomic force microscopy after the application of anodic potentials and found subtle changes in surface morphology around step edges, and also over the basal surface at a density similar to that estimated for point defects (see Supporting Information, section S4),^{49, 50} suggesting these locations (particularly step edges) as possible sites for ion intercalation/de-intercalation.

The reduction peak of the CVs was integrated to produce the charge transferred and the charge density, which is the ratio of charge to the droplet contact area (measured at the de-

intercalation potential). The values were plotted against the upper potential limit of CVs, as shown in Figure 5. The charge density of the reduction peak increases more or less linearly with the upper limit of CV (and hence time). The surface concentration of ClO_4^- intercalated into AM HOPG can also be obtained, considering the one electron process of intercalation/de-intercalation (see eqn.(1)). The CV with the upper limit of +2 V leads to a surface concentration of 31 pmol cm^{-2} , accounting for 0.5% of the carbon atoms in the top graphene layer. This value is of similar magnitude to the step edge density on AM grade graphite (0.09%),¹⁹ indicating that the extent of the intercalation process causing the electrowetting is rather subtle.

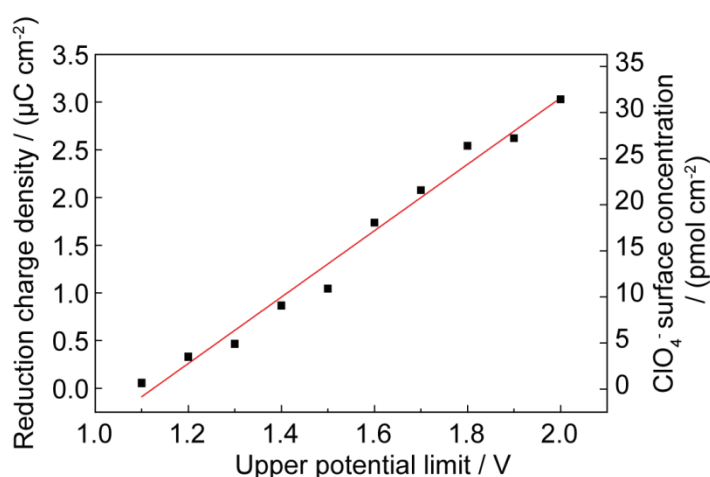


Figure 5. Charge density for the reduction peak of the CVs carried out in different potential ranges (1 V s^{-1}), and corresponding ClO_4^- surface concentration, plotted as a function of upper potential limit.

XPS measurements were carried out to characterize the compositions of AM HOPG surfaces. In the high-resolution XPS Cl 2p spectrum of the electrochemically-treated AM HOPG sample (Figure 6), a pronounced peak at a binding energy of 206.9 eV was observed,

corresponding to the Cl 2p_{3/2} component arising from the intercalated perchlorate ions.⁴⁴ A second bonding environment was also observed, possessing a Cl 2p_{3/2} component at a binding energy of 208.3 eV and was attributed to adsorbed ClO₄⁻.⁵¹ The associated Cl 2p_{1/2} components were found to be at 208.5 eV (intercalated) and 209.9 eV (adsorbed). On the sample without electrochemical treatment, only adsorbed perchlorate ions (207.9 eV and 209.5 eV) were observed, along with a small amount of remnant NaClO₄ (209.3 eV and 210.9 eV) from removing the electrolyte droplet; see Supporting Information, section S5. The quantity of Cl was found to be significantly higher on the electrochemically-treated HOPG sample, compared with that of the control sample. These data confirm the intercalation of ClO₄⁻ ions into AM HOPG structure at relatively high anodic potentials, where electrowetting occurs. We believe this is the main effect causing electrowetting, although there may be some contribution from adsorbed ClO₄⁻, which may adsorb on HOPG.⁴⁴

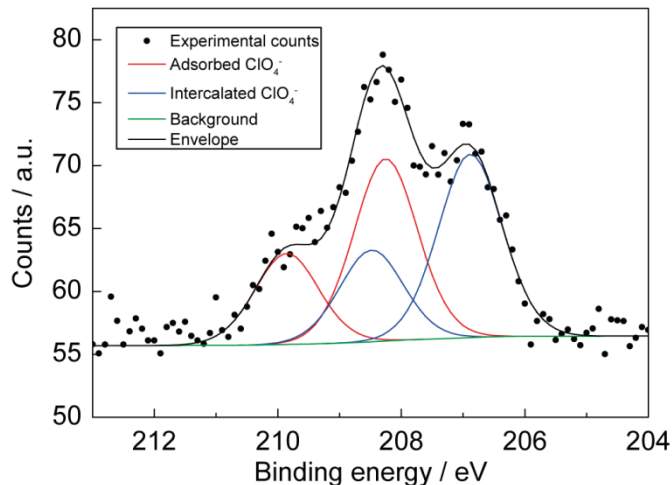


Figure 6. XPS spectrum of the Cl 2p region on electrochemically-treated AM HOPG (30 CVs swept from 0 to +2 V at 1 V s⁻¹, with the potential then held at +1.5 V for 30 s), using a droplet of 1 mM NaClO₄. The spectrum has been fitted with peaks for different species as indicated in the figure. The sum of fitting curves (black solid line) is consistent with the raw data (black dots).

Scan rate effect on electrowetting

The influence of timescale on the intercalation/de-intercalation of ClO_4^- (1 mM NaClO_4) and electrowetting of the droplet was investigated on AM HOPG by comparing scan rates of 0.1, 0.3 and 1 V s^{-1} . Electrowetting behavior was observed on HOPG at all scan rates employed, but to different extents. As shown in the examples in Figure 7a, when a slow scan rate (0.1 V s^{-1}) was employed, the CA for the droplet at a potential of +0.92 V on the forward scan (oxidation) was 34°. A CA of 42° at +0.96 V (on the forward scan) was obtained for the intermediate scan rate (0.3 V s^{-1}). As the scan rate was increased to 1 V s^{-1} , a CA of 44° at +1.09 V (on the forward scan) was obtained. Thus, even though the potential is increasingly higher in this series of images, the scan rate (timescale) has a significant effect. In fact, the corresponding CV responses show that the reduction peak (de-intercalation) shifted negatively, while the oxidation peak (intercalation) shifted positively, and both became less pronounced, with increasing scan rate. The corresponding intercalation charges were 61 nC (0.1 V s^{-1}), 1.8 nC (0.3 V s^{-1}) and 0.5 nC (1 V s^{-1}). At slow scan rates, the intercalation/de-intercalation process clearly occurs more extensively at the HOPG substrate. As a result, a minimum CA of 18° was obtained for the droplet with the CV swept at 0.1 V s^{-1} , compared to that of 20° and 25° for 0.3 and 1 V s^{-1} , respectively (Figure 7b). Moreover, the electrowetting process follows the CV response more faithfully at slow scan rate, leading to a smaller hysteresis of CA between the forward and reverse sweeps.

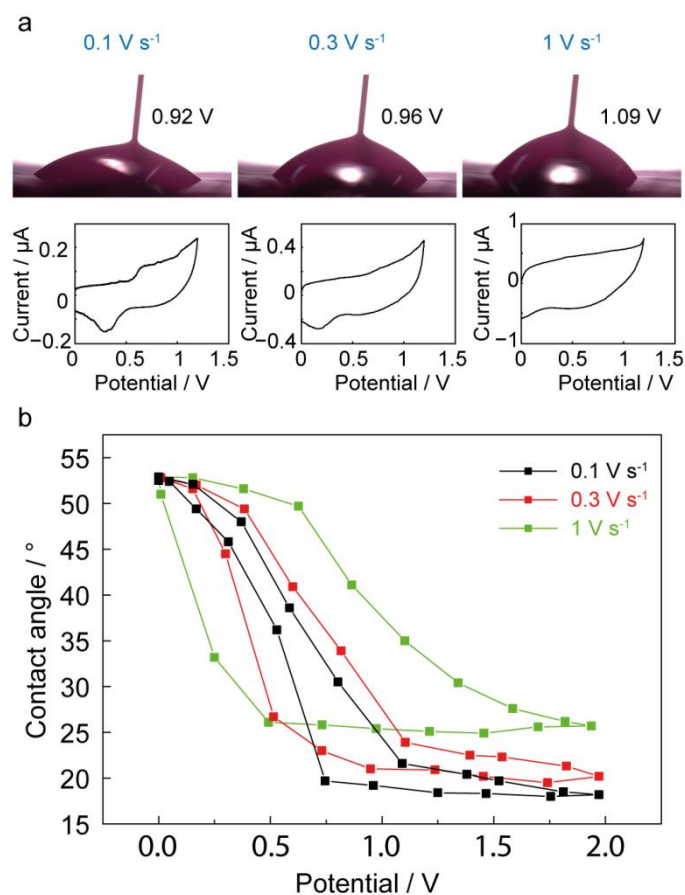


Figure 7. (a) Snapshots for droplet electrowetting of 1 mM NaClO₄ solution on AM HOPG during the forward scan of a cyclic voltammogram in the potential range of 0~+1.2 V, with scan rates of 0.1, 0.3 and 1 V s⁻¹. The potentials at which the snapshots were taken are indicated and the full cyclic voltammograms are shown below. (b) Contact angle of a 1 mM NaClO₄ droplet on AM HOPG plotted against the potential, during CV measurements from 0 to + 2 V at scan rates of 0.1, 0.3 and 1 V s⁻¹.

It should be noted that in some cases the droplet could detach from the CE/RE due to the significant electrowetting on AM HOPG at positive potentials. In this situation, the HOPG surface is at the open-circuit potential, yet a low CA and high RCD were found to be maintained. This is excellent evidence that electrochemically driven intercalation is

responsible for the electrowetting. When the cell connection was re-made by moving the CE/RE down into the spread droplet (at 0 V), de-intercalation occurs and the droplet recovered its original morphology (see Supporting Information, section S6).

Potential polarity effect on electrowetting

When CV potential scanning was in the cathodic window with AM HOPG, no obvious changes in CA and RCD of droplet were observed (see Supporting Information, section S7), with the same concentration (1 mM) of NaClO₄ solution used. The CA only varied by 2° at most during the CV and the RCD was more or less stable. Thus, electrowetting of the aqueous droplet on HOPG only occurred at positive potentials. This behavior is in agreement with a study of electrowetting of carbon nanotube membranes,⁵² although the effect in that case was attributed to electrochemistry of oxygen-containing surface functional groups. That we only observe electrowetting in the positive potential region, means that the mechanism is different from the EWOD, which is only weakly dependent on the polarity of potential applied, and tends to follow the Young-Lippmann equation.^{4, 7, 12}

Substrate effect on electrowetting

As the (electro-)wetting of a substrate by a droplet can be affected by the roughness of the substrate,^{18, 53, 54} some droplet cell experiments (1 mM NaClO₄) were also conducted on the surface of SPI-3 grade HOPG, which has more than 2 orders of magnitude more step edges (density) than AM (Figure 1b), with a predominance of multilayer rather than monolayer step edges.^{19, 27, 30, 31} This leads to higher roughness of SPI-3. According to Wenzel model:^{53, 54}

$$\cos \theta_r = r \cos \theta_0 \quad \text{eqn. (2)}$$

where θ_r and θ_0 are the CA on a rough surface and a flat surface, respectively, and r is the surface roughness, defined as the ratio of the actual area of the rough surface to the geometric

projected area, one might expect the CA on AM HOPG to be larger than for SPI-3 HOPG at all potentials. However, in contrast to the observations on AM HOPG during CV scanning, only a small amount electrowetting of the droplet was seen on SPI-3 (Figure 8). A decrease of 6° in CA was obtained during the scan from 0 to +2 V, while an increase of 4.5% was seen for RCD at a scan rate of 1 V s⁻¹(compare Figure 8 with Figure 2c). This is a very striking difference in behavior.

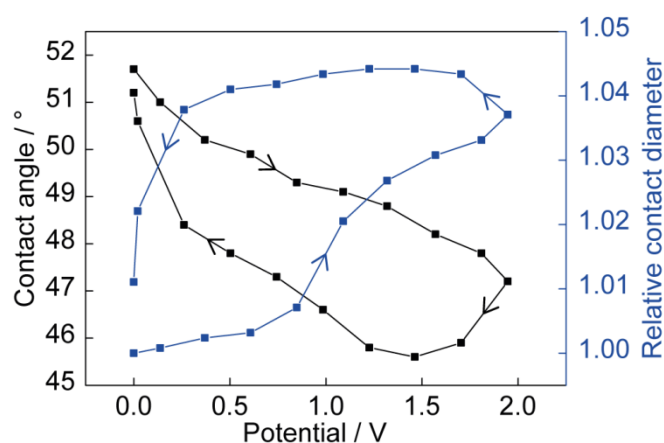


Figure 8. Contact angle and relative contact diameter of electrowetting for a droplet of 1 mM NaClO₄ solution at the surface of SPI-3 HOPG plotted against the potentials of a CV carried out in the range of 0~2 V, with a scan rate of 1 V s⁻¹.

A total of 20 repetitive CVs between 0 and +2 V (1 V s⁻¹) were carried out on the freshly cleaved surface of each grade of HOPG, to resolve possible electrochemical reactions, with the resulting voltammograms shown in Figure 9. On AM HOPG, we observe the development of the cathodic potential peaks that we described earlier, and the anodic oxidation process at the most positive potentials >+1.5 V. In contrast, even over 20

successive scans for SPI-3 HOPG, only the anodic current at $>+1.5\text{V}$ was discernible, with little evidence of ion intercalation/de-intercalation. This result, over the potential range shown, is important as it further confirms that the oxidation process at $>+1.5\text{ V}$ are not the dominant factor in droplet electrowetting of AM HOPG.

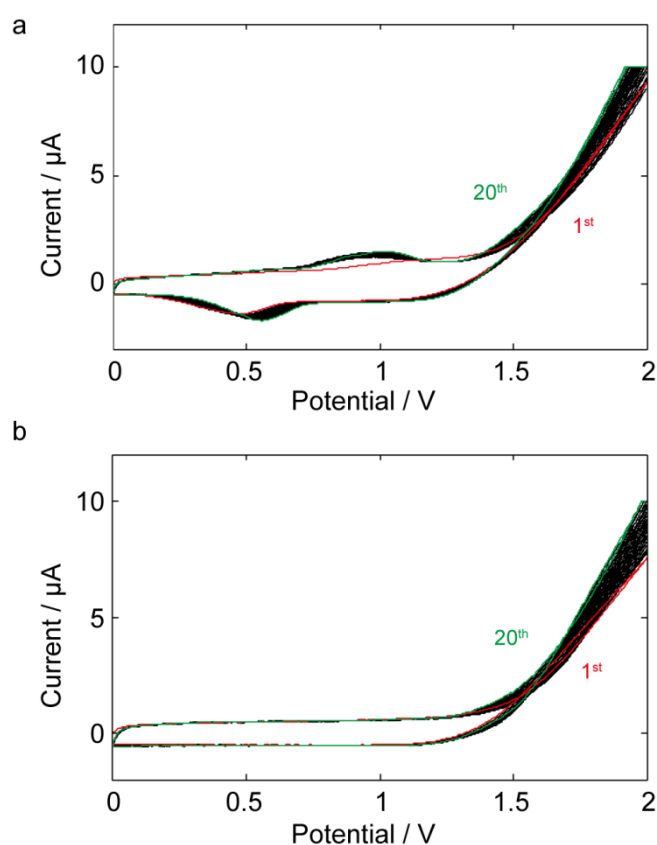


Figure 9. Twenty repetitive cyclic voltammograms for a droplet of 1 mM NaClO_4 solution on (a) AM grade and (b) SPI-3 grade HOPG, recorded in the potential range of 0~+2 V, at a scan rate of 1 V s^{-1} .

We attribute the difference in the electrochemical responses of these two grades of HOPG to the feasibility (or not) of intercalation/de-intercalation processes. The intercalation of ions

requires sufficient energy to overcome the van de Waals forces that hold the graphene layers together in graphite. The energy increases with the number of adjacent graphene layers.^{44, 45} Since AM HOPG has low step edge coverage of monoatomic steps,^{19, 27} as illustrated schematically in Figure 10a, ClO_4^- ions can be relatively easily inserted into the graphene layers of AM HOPG through the (exposed) step edges during the forward scan of CV (oxidation), which are negatively charged atop a neutral underlying basal surface.^{29, 55} The intercalation produces enhanced electrowetting of the droplet on graphite through the introduction of oxygen-containing ions (ClO_4^-). As the scan number is increased, the intercalation/de-intercalation of ClO_4^- becomes easier, causing the reduction peak to shift to positive potentials, for example, as described above. Compared with AM HOPG, SPI-3 HOPG has many more step edges that are predominantly multiple layers.^{30, 31} This greatly enhances the binding force between the graphene layers, leading to less delamination of step edges with time.⁵⁶ Moreover, anion intercalation would be hindered by strong repulsive coulombic forces, due to the large amount of negative charges at the multilayer step edges.^{29, 55} As a result, considerably more energy is required for the intercalation of ClO_4^- ions into SPI-3 HOPG, making it less vulnerable to the attack of ClO_4^- anions (Figure 10b). This mechanism can also be used to explain the asymmetry of the electrowetting droplet observed occasionally in some cases (Figure 3), as the step edge density and arrangement on AM HOPG, is non-uniform¹⁹ and determined by the cleavage.

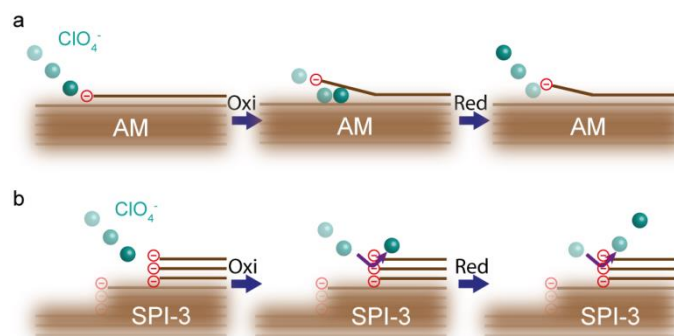


Figure 10. Schematic depicting the pathway of ClO_4^- under CV conditions anodically for (a) AM HOPG, leading to the intercalation (oxidation) and de-intercalation (reduction) processes at monolayer step edges and (b) SPI-3 HOPG, where little intercalation/de-intercalation of ClO_4^- occurs at multilayer step edges (not to scale). Note that negative charges at step edges (oxygen-containing moieties) are marked in red.

Anion effect on electrowetting

There have been considerable efforts to study anion intercalation into graphite, so as to elucidate the intercalating properties of different types of anions.^{21, 23} Considering the relationship between intercalation and electrowetting that we have described, we found that similar effects to those reported above for ClO_4^- were found with SO_4^{2-} , with a typical response of contact angle and relative contact diameter versus potential in 1 mM Na_2SO_4 solution shown in Figure 11. The corresponding CV is shown in Supporting Information, section S8. However, two other types of much larger anions, $\text{H}_2\text{PO}_4^-/\text{HPO}_4^{2-}$ and fluorescein dianion, with a concentration of 1 mM, were also briefly considered on AM HOPG during CV measurements. Experiments were conducted in the same potential range as for ClO_4^- (i.e. 0~+2 V vs Ag/AgCl). We found the droplet containing $\text{H}_2\text{PO}_4^-/\text{HPO}_4^{2-}$ did not electrowet AM HOPG surface, in line with other studies.²¹ In the case of fluorescein, the droplet was shown

to maintain its shape under the potentials applied and no electrowetting was observed. The corresponding CVs demonstrated no oxidation and reduction peaks for intercalation and de-intercalation of ions (see Supporting Information, section S8).

This study further confirms that ion-intercalation/de-intercalation of specific ions (ClO_4^-), rather than the anodic formation of graphite oxide or, water oxidation is responsible for the electrowetting of graphite that we observe.

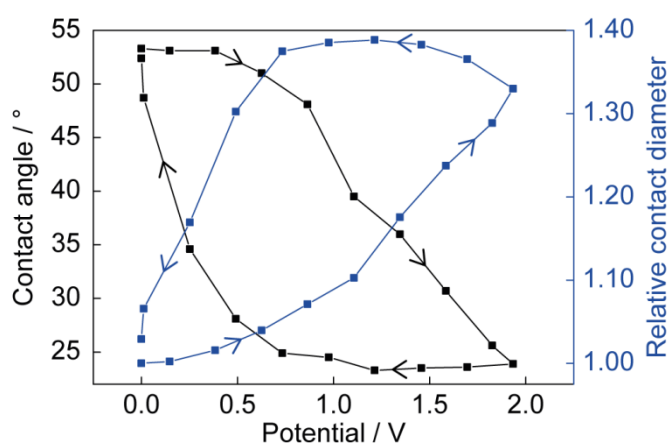


Figure 11. Contact angle and relative contact diameter of electrowetting for a droplet of 1 mM Na_2SO_4 solution at the surface of AM HOPG plotted against the potentials of a CV carried out in the range of 0~+2 V, with a scan rate of 1 V s^{-1} .

Conclusions

We have demonstrated a new mechanism for electrowetting based on ClO_4^- (and SO_4^{2-}) intercalation/de-intercalation into step edges on the basal surface of HOPG. Intercalation/de-intercalation of ClO_4^- (and SO_4^{2-}) in the top graphene layers of graphite surfaces, induces changes in local surface morphology and charge that alters the wettability of the substrate by

the droplet. Electrowetting occurs at moderate positive potentials under CV conditions where ClO_4^- intercalation occurs. The slowest scan rate investigated (0.1 V s^{-1}) leads to more significant intercalation which enhances the electrowetting behavior. Little electrowetting of NaClO_4 was seen on SPI-3 HOPG, as the energy to expand the gaps between graphene layers is greatly enhanced by the strong binding force imposed by the high-density of multilayer step edges.

The work we have presented shows that electrochemistry can be used as a powerful means for tailoring the surface properties of graphite and manipulating the movement of a droplet on it. The possibility of using ion intercalation/de-intercalation to introduce significant, reversible and repeatable electrowetting phenomena on a reasonable timescale opens up new prospects for low voltage electrowetting devices based on layered materials and/or ion intercalation/de-intercalation that do not require an EWOD format.

Associated content

Supporting Information

A movie ('Electrowetting of AM HOPG') showing the electrowetting of AM HOPG by a droplet of 1 mM NaClO_4 solution during the CV swept from 0 V to +2 V at a scan rate of 1 V s^{-1} .

S1 - Electrowetting of a droplet of 0.1 M NaClO_4 solution on AM HOPG

S2 - Electrowetting of a droplet of 1 mM NaClO_4 solution on AM HOPG under repetitive cyclic scans

S3 - Cyclic voltammograms of a droplet of 1 mM NaClO_4 solution on AM HOPG

S4 - Atomic force microscopy images of AM HOPG after the removal of droplet

S5 - X-ray photoelectron spectroscopy measurement of AM HOPG control sample

S6 - Electrowetting of a droplet of 1 mM NaClO₄ solution on HOPG with the electric circuit on and off

S7 - Potential polarity effect on the electrowetting of a droplet of 1 mM NaClO₄ solution on AM HOPG

S8 - Cyclic voltammograms of a droplet containing 1 mM Na₂SO₄, Na₃PO₄ or sodium fluorescein on AM HOPG

Author information

Corresponding author

*E-mail: p.r.unwin@warwick.ac.uk.

Notes

The authors declare no competing financial interest.

Acknowledgment

This work was funded by the European Research Council (ERC-2009-AdG 247143-QUANTIF). G.Z acknowledges support by a Chancellor's International Scholarship at the University of Warwick. We are particularly grateful to Kim McKelvey, Ashley Page and Minkyung Kang for LabVIEW support and programming. The Omicron Multiprobe used for XPS studies in this research was funded through the Science Cities Advanced Materials Project 1: Creating and Characterising Next Generation of Advanced Materials with support from Advantage West Midlands and the European Regional Development Fund.

References

1. Frysalı, M. A.; Papoutsakis, L.; Kenanakis, G.; Anastasiadis, S. H. Functional Surfaces with Photocatalytic Behavior and Reversible Wettability: ZnO Coating on Silicon Spikes. *J. Phys. Chem. C* **2015**, *119* (45), 25401-25407.
2. Xu, L.; Liu, N.; Cao, Y.; Lu, F.; Chen, Y.; Zhang, X.; Feng, L.; Wei, Y. Mercury Ion Responsive Wettability and Oil/Water Separation. *ACS Appl. Mater. Interfaces* **2014**, *6* (16), 13324-13329.
3. Chowdhury, D.; Maoz, R.; Sagiv, J. Wetting Driven Self-Assembly as a New Approach to Template-Guided Fabrication of Metal Nanopatterns. *Nano Lett.* **2007**, *7* (6), 1770-1778.
4. Paneru, M.; Priest, C.; Sedev, R.; Ralston, J. Static and Dynamic Electrowetting of an Ionic Liquid in a Solid/Liquid/Liquid System. *J. Am. Chem. Soc.* **2010**, *132* (24), 8301-8308.
5. Kornyshev, A. A.; Kucernak, A. R.; Marinescu, M.; Monroe, C. W.; Sleightholme, A. E. S.; Urbakh, M. Ultra-Low-Voltage Electrowetting. *J. Phys. Chem. C* **2010**, *114* (35), 14885-14890.
6. Taherian, F.; Leroy, F.; van der Vegt, N. F. A. Interfacial Tension Does Not Drive Asymmetric Nanoscale Electrowetting on Graphene. *Langmuir* **2015**, *31* (16), 4686-4695.
7. Ricks-Laskoski, H. L.; Snow, A. W. Synthesis and Electric Field Actuation of an Ionic Liquid Polymer. *J. Am. Chem. Soc.* **2006**, *128* (38), 12402-12403.
8. Hayes, R. A.; Feenstra, B. J. Video-Speed Electronic Paper Based on Electrowetting. *Nature* **2003**, *425* (6956), 383-385.
9. Kuiper, S.; Hendriks, B. H. W. Variable-Focus Liquid Lens for Miniature Cameras. *Appl. Phys. Lett.* **2004**, *85* (7), 1128-1130.
10. Yeo, L.; Friend, J. Electrowetting, Applications. In *Encyclopedia of Microfluidics and Nanofluidics*, Li, D., Ed.; Springer US, 2014, pp 1-14.
11. Yeo, L. Y.; Chang, H.-C. Electrowetting Films on Parallel Line Electrodes. *Phys. Rev. E* **2006**, *73* (1), 011605.
12. Klarman, D.; Andelman, D.; Urbakh, M. A Model of Electrowetting, Reversed Electrowetting, and Contact Angle Saturation. *Langmuir* **2011**, *27* (10), 6031-6041.
13. Bhushan, B.; Pan, Y. Role of Electric Field on Surface Wetting of Polystyrene Surface. *Langmuir* **2011**, *27* (15), 9425-9429.

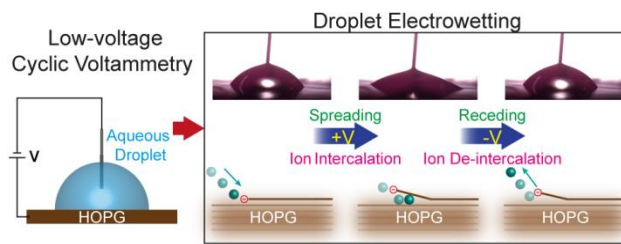
14. Restolho, J.; Mata, J. L.; Saramago, B. Electrowetting of Ionic Liquids: Contact Angle Saturation and Irreversibility. *J. Phys. Chem. C* **2009**, *113* (21), 9321-9327.
15. Annapragada, S. R.; Dash, S.; Garimella, S. V.; Murthy, J. Y. Dynamics of Droplet Motion under Electrowetting Actuation. *Langmuir* **2011**, *27* (13), 8198-8204.
16. Chen, L.; Li, C.; van der Vegt, N. F. A.; Auernhammer, G. K.; Bonaccorso, E. Initial Electrospreading of Aqueous Electrolyte Drops. *Phys. Rev. Lett.* **2013**, *110* (2), 026103.
17. Liu, Y.; Liang, Y.-E.; Sheng, Y.-J.; Tsao, H.-K. Ultralow Voltage Irreversible Electrowetting Dynamics of an Aqueous Drop on a Stainless Steel Surface. *Langmuir* **2015**, *31* (13), 3840-3846.
18. Pu, J.; Wan, S.; Lu, Z.; Zhang, G.-a.; Wang, L.; Zhang, X.; Xue, Q. Controlled Water Adhesion and Electrowetting of Conducting Hydrophobic Graphene/Carbon Nanotubes Composite Films on Engineering Materials. *J. Mater. Chem. A* **2013**, *1* (4), 1254-1260.
19. Patel, A. N.; Collignon, M. G.; O'Connell, M. A.; Hung, W. O.; McKelvey, K.; Macpherson, J. V.; Unwin, P. R. A New View of Electrochemistry at Highly Oriented Pyrolytic Graphite. *J. Am. Chem. Soc.* **2012**, *134* (49), 20117-20130.
20. Yoon, G.; Seo, D.-H.; Ku, K.; Kim, J.; Jeon, S.; Kang, K. Factors Affecting the Exfoliation of Graphite Intercalation Compounds for Graphene Synthesis. *Chem. Mater.* **2015**, *27* (6), 2067-2073.
21. Hathcock, K. W.; Brumfield, J. C.; Goss, C. A.; Irene, E. A.; Murray, R. W. Incipient Electrochemical Oxidation of Highly Oriented Pyrolytic Graphite: Correlation between Surface Blistering and Electrolyte Anion Intercalation. *Anal. Chem.* **1995**, *67* (13), 2201-2206.
22. Alsmeyer, D. C.; McCreery, R. L. In Situ Raman Monitoring of Electrochemical Graphite Intercalation and Lattice Damage in Mild Aqueous Acids. *Anal. Chem.* **1992**, *64* (14), 1528-1533.
23. Noel, M.; Santhanam, R. Electrochemistry of Graphite Intercalation Compounds. *J. Power Sources* **1998**, *72* (1), 53-65.
24. Hui, J.; Burgess, M.; Zhang, J.; Rodriguez-Lopez, J. Layer Number Dependence of Li(+) Intercalation on Few-Layer Graphene and Electrochemical Imaging of Its Solid-Electrolyte Interphase Evolution. *ACS Nano* **2016**, *10* (4), 4248-4257.
25. Weast, R. C. *CRC Handbook of Chemistry and Physics*; 64th ed.; CRC Press: Boca Raton, Florida, 1983.

26. Kirkman, P. M.; Güell, A. G.; Cuharuc, A. S.; Unwin, P. R. Spatial and Temporal Control of the Diazonium Modification of sp² Carbon Surfaces. *J. Am. Chem. Soc.* **2014**, *136* (1), 36-39.
27. Zhang, G.; Kirkman, P. M.; Patel, A. N.; Cuharuc, A. S.; McKelvey, K.; Unwin, P. R. Molecular Functionalization of Graphite Surfaces: Basal Plane versus Step Edge Electrochemical Activity. *J. Am. Chem. Soc.* **2014**, *136* (32), 11444-11451.
28. Zhang, G.; Cuharuc, A. S.; Güell, A. G.; Unwin, P. R. Electrochemistry at Highly Oriented Pyrolytic Graphite (HOPG): Lower Limit for the Kinetics of Outer-sphere Redox Processes and General Implications for Electron Transfer Models. *Phys. Chem. Chem. Phys.* **2015**, *17* (17), 11827-11838.
29. Lai, S. C. S.; Patel, A. N.; McKelvey, K.; Unwin, P. R. Definitive Evidence for Fast Electron Transfer at Pristine Basal Plane Graphite from High-Resolution Electrochemical Imaging. *Angew. Chem. Int. Ed.* **2012**, *51* (22), 5405-5408.
30. Patel, A. N.; Tan, S. Y.; Unwin, P. R. Epinephrine Electro-Oxidation Highlights Fast Electrochemistry at the Graphite Basal Surface. *Chem. Commun.* **2013**, *49* (78), 8776-8778.
31. Patel, A. N.; Tan, S. Y.; Miller, T. S.; Macpherson, J. V.; Unwin, P. R. Comparison and Reappraisal of Carbon Electrodes for the Voltammetric Detection of Dopamine. *Anal. Chem.* **2013**, *85* (24), 11755-11764.
32. Cuharuc, A. S.; Zhang, G.; Unwin, P. R. Electrochemistry of Ferrocene Derivatives on Highly Oriented Pyrolytic Graphite (HOPG): Quantification and Impacts of Surface Adsorption. *Phys. Chem. Chem. Phys.* **2016**, *18* (6), 4966-4977.
33. Williams, C. G.; Edwards, M. A.; Colley, A. L.; Macpherson, J. V.; Unwin, P. R. Scanning Micropipet Contact Method for High-Resolution Imaging of Electrode Surface Redox Activity. *Anal. Chem.* **2009**, *81* (7), 2486-2495.
34. McHale, G.; Rowan, S. M.; Newton, M. I.; Banerjee, M. K. Evaporation and the Wetting of a Low-Energy Solid Surface. *J. Phys. Chem. B* **1998**, *102* (11), 1964-1967.
35. Li, Z.; Wang, Y.; Kozbial, A.; Shenoy, G.; Zhou, F.; McGinley, R.; Ireland, P.; Morganstein, B.; Kunkel, A.; Surwade, S. P.; Li, L.; Liu, H. Effect of Airborne Contaminants on the Wettability of Supported Graphene and Graphite. *Nat. Mater.* **2013**, *12* (10), 925-931.
36. Ashraf, A.; Wu, Y.; Wang, M. C.; Aluru, N. R.; Dastgheib, S. A.; Nam, S. Spectroscopic Investigation of the Wettability of Multilayer Graphene Using Highly Ordered Pyrolytic Graphite as a Model Material. *Langmuir* **2014**, *30* (43), 12827-12836.

37. Schrader, M. E. Ultrahigh-Vacuum Techniques in the Measurement of Contact Angles. 5. LEED Study of the Effect of Structure on the Wettability of Graphite. *J. Phys. Chem.* **1980**, *84* (21), 2774-2779.
38. Hong, S.-J.; Li, Y.-F.; Hsiao, M.-J.; Sheng, Y.-J.; Tsao, H.-K. Anomalous Wetting on a Superhydrophobic Graphite Surface. *Appl. Phys. Lett.* **2012**, *100* (12), 121601.
39. Wei, Y.; Jia, C. Q. Intrinsic Wettability of Graphitic Carbon. *Carbon* **2015**, *87*, 10-17.
40. Kozbial, A.; Li, Z.; Sun, J.; Gong, X.; Zhou, F.; Wang, Y.; Xu, H.; Liu, H.; Li, L. Understanding the Intrinsic Water Wettability of Graphite. *Carbon* **2014**, *74*, 218-225.
41. Hung, S.-W.; Hsiao, P.-Y.; Chen, C.-P.; Chieng, C.-C. Wettability of Graphene-Coated Surface: Free Energy Investigations Using Molecular Dynamics Simulation. *J. Phys. Chem. C* **2015**, *119* (15), 8103-8111.
42. Walker, E. K.; Vanden Bout, D. A.; Stevenson, K. J. Spectroelectrochemical Investigation of an Electrogenerated Graphitic Oxide Solid–Electrolyte Interphase. *Anal. Chem.* **2012**, *84* (19), 8190-8197.
43. Choo, H.-S.; Kinumoto, T.; Nose, M.; Miyazaki, K.; Abe, T.; Ogumi, Z. Electrochemical Oxidation of Highly Oriented Pyrolytic Graphite during Potential Cycling in Sulfuric Acid Solution. *J. Power Sources* **2008**, *185* (2), 740-746.
44. Schnyder, B.; Alliata, D.; Kötz, R.; Siegenthaler, H. Electrochemical Intercalation of Perchlorate Ions in HOPG: an SFM/LFM and XPS Study. *Appl. Surf. Sci.* **2001**, *173* (3–4), 221-232.
45. Alliata, D.; Kötz, R.; Haas, O.; Siegenthaler, H. In Situ AFM Study of Interlayer Spacing during Anion Intercalation into HOPG in Aqueous Electrolyte. *Langmuir* **1999**, *15* (24), 8483-8489.
46. Goss, C. A.; Brumfield, J. C.; Irene, E. A.; Murray, R. W. Imaging the Incipient Electrochemical Oxidation of Highly Oriented Pyrolytic Graphite. *Anal. Chem.* **1993**, *65* (10), 1378-1389.
47. Parvez, K.; Wu, Z.-S.; Li, R.; Liu, X.; Graf, R.; Feng, X.; Müllen, K. Exfoliation of Graphite into Graphene in Aqueous Solutions of Inorganic Salts. *J. Am. Chem. Soc.* **2014**, *136* (16), 6083-6091.
48. Parvez, K.; Li, R.; Puniredd, S. R.; Hernandez, Y.; Hinkel, F.; Wang, S.; Feng, X.; Müllen, K. Electrochemically Exfoliated Graphene as Solution-Processable, Highly Conductive Electrodes for Organic Electronics. *ACS Nano* **2013**, *7* (4), 3598-3606.

49. Chang, H.; Bard, A. J. Scanning Tunneling Microscopy Studies of Carbon-Oxygen Reactions on Highly Oriented Pyrolytic Graphite. *J. Am. Chem. Soc.* **1991**, *113* (15), 5588-5596.
50. Chang, H.; Bard, A. J. Formation of Monolayer Pits of Controlled Nanometer Size on Highly Oriented Pyrolytic Graphite by Gasification Reactions as Studied by Scanning Tunneling Microscopy. *J. Am. Chem. Soc.* **1990**, *112* (11), 4598-4599.
51. Moulder, J. F.; Stickle, W. F.; Sobol, P. E.; Bomben, K. D. *Handbook of X-ray Photoelectron Spectroscopy*; Physical Electronics Division, Perkin-Elmer Corporation: Eden Prairie, MN, 1992.
52. Wang, Z.; Ci, L.; Chen, L.; Nayak, S.; Ajayan, P. M.; Koratkar, N. Polarity-Dependent Electrochemically Controlled Transport of Water through Carbon Nanotube Membranes. *Nano Lett.* **2007**, *7* (3), 697-702.
53. Han, Z.; Tay, B.; Tan, C.; Shakerzadeh, M.; Ostrikov, K. Electrowetting Control of Cassie-to-Wenzel Transitions in Superhydrophobic Carbon Nanotube-Based Nanocomposites. *ACS Nano* **2009**, *3* (10), 3031-3036.
54. Shirtcliffe, N. J.; McHale, G.; Newton, M. I.; Perry, C. C. Wetting and Wetting Transitions on Copper-Based Super-Hydrophobic Surfaces. *Langmuir* **2005**, *21* (3), 937-943.
55. Koestner, R.; Roiter, Y.; Kozhinova, I.; Minko, S. Effect of Local Charge Distribution on Graphite Surface on Nafion Polymer Adsorption as Visualized at the Molecular Level. *J. Phys. Chem. C* **2011**, *115* (32), 16019-16026.
56. Güell, A. G.; Cuharuc, A. S.; Kim, Y. R.; Zhang, G.; Tan, S. Y.; Ebejer, N.; Unwin, P. R. Redox-Dependent Spatially Resolved Electrochemistry at Graphene and Graphite Step Edges. *ACS Nano* **2015**, *9* (4), 3558-3571.

Table of Contents



Supporting Information

Low-voltage Voltammetric Electrowetting of Graphite Surfaces by Ion Intercalation/De-intercalation

Guohui Zhang,[†] Marc Walker[‡] and Patrick R. Unwin^{*†}

[†] Department of Chemistry, University of Warwick, Coventry, CV4 7AL, United Kingdom.

[‡] Department of Physics, University of Warwick, Coventry CV4 7AL, United Kingdom.

* To whom correspondence should be addressed. Email: p.r.unwin@warwick.ac.uk.

Contents

S1 Electrowetting of a droplet of 0.1 M NaClO ₄ solution on AM HOPG	Page S-3
S2 Electrowetting of a droplet of 1 mM NaClO ₄ solution on AM HOPG under repetitive cyclic scans	Page S-4
S3 Cyclic voltammograms of a droplet of 1 mM NaClO ₄ solution on AM HOPG	Page S-5
S4 Atomic force microscopy images of AM HOPG after the removal of droplet	Page S-6
S5 X-ray photoelectron spectroscopy measurement of AM HOPG control sample	Page S-7
S6 Electrowetting of a droplet of 1 mM NaClO ₄ solution on HOPG with the electric circuit on and off	Page S-8

S7 | Potential polarity effect on the electrowetting of a droplet of 1 mM NaClO₄ solution on AM HOPG Page S-9

S8 | Cyclic voltammograms of a droplet containing 1 mM Na₂SO₄, Na₃PO₄ or sodium fluorescein on AM HOPG Page S-10

References Page S-12

S1 | Electrowetting of a droplet of 0.1 M NaClO₄ solution on AM HOPG

For comparison with the data in the manuscript which focused on 1 mM NaClO₄, a droplet of 0.1 M NaClO₄ solution on AM HOPG was tested using a CV scanned from 0 V to +2 V (at 1 V s⁻¹). Similar electrowetting behavior to that for the concentration of 1 mM was observed, as evident from the changes in contact angle and relative contact diameter against potential applied, as shown in Figure S1.

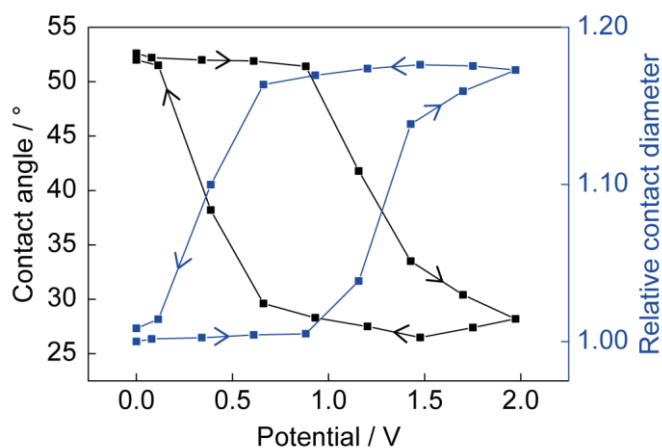


Figure S1 Contact angle and relative contact diameter for a droplet of 0.1 M NaClO₄ aqueous solution at the surface of AM HOPG, during a cyclic voltammogram recorded in the potential range of 0 V to +2 V, at a scan rate of 1 V s⁻¹.

S2 | Electrowetting of a droplet of 1 mM NaClO₄ solution on AM HOPG under repetitive cyclic scans

A total of 20 continuous CVs were carried out from 0 V to +2 V, with a droplet of 1 mM NaClO₄ solution on AM HOPG, at a scan rate of 1 V s⁻¹. It was found that the electrowetting behavior was very repeatable after 5 cyclic scans onwards (Figure S2), and the hysteresis of contact angle was reduced, compared with that for the first cycle which required a higher potential to introduce the wetting.

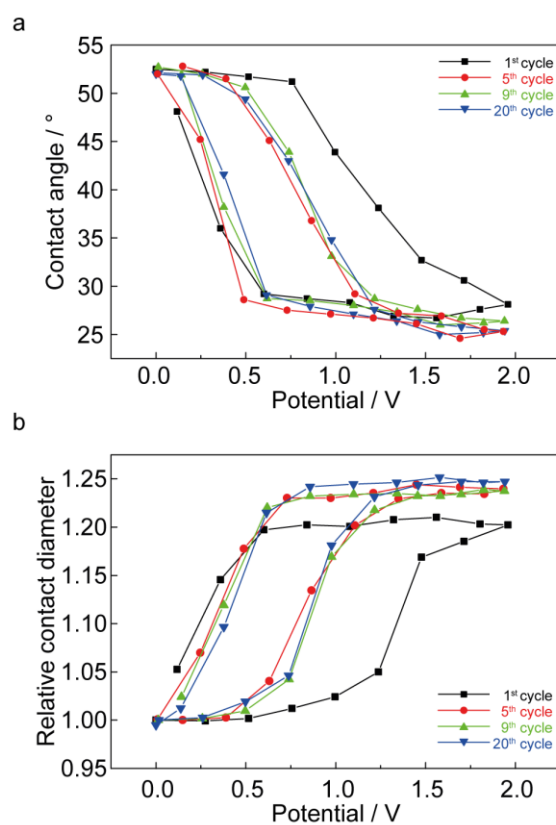


Figure S2. (a) Contact angle and (b) relative contact diameter of electrowetting for a droplet of 1 mM NaClO₄ solution on AM HOPG, during the 1st, 5th, 9th and 20th cycles of 20 repetitive scans (from 0 to +2 V, 1 V s⁻¹).

S3 | Cyclic voltammograms of a droplet of 1 mM NaClO₄ solution on AM HOPG

In addition to Figure 4 in the main text, other CV responses over different potential windows for a droplet of 1 mM NaClO₄ solution on AM HOPG are shown in Figure S3. With an increase of the upper potential limit, the reduction peak on the reverse scan became more developed and shifted towards more positive potentials.

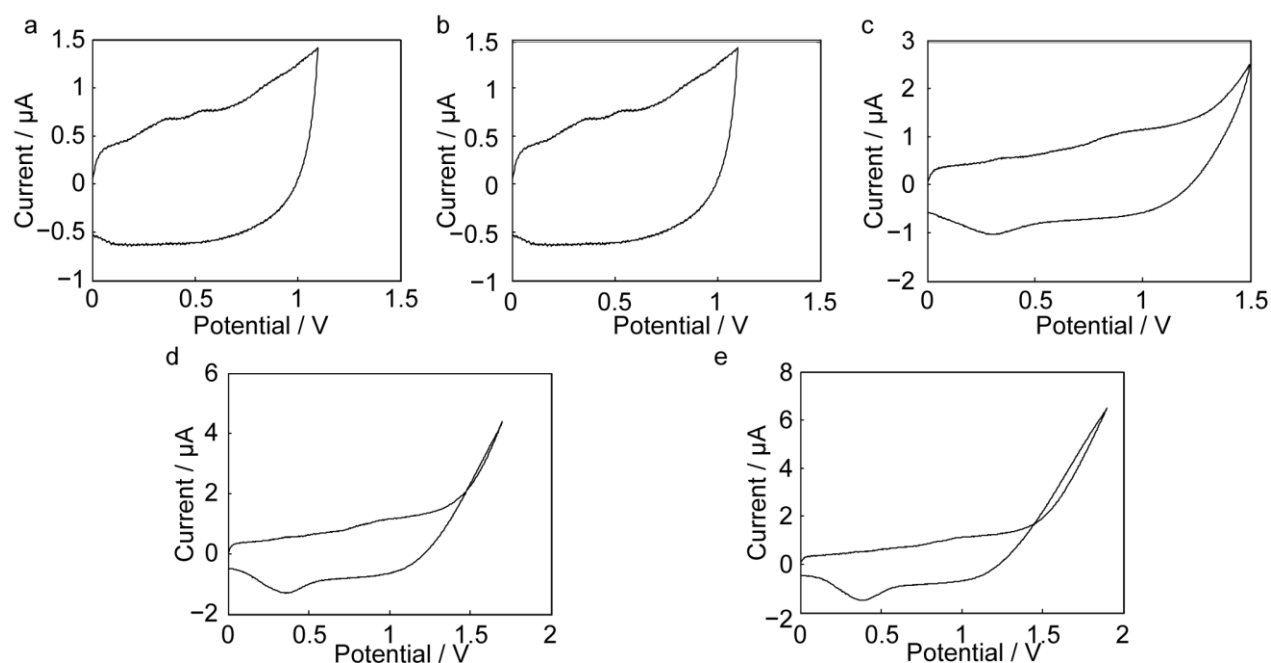


Figure S3. Cyclic voltammograms for a droplet of 1 mM NaClO₄ solution (on AM grade HOPG) with the voltage swept in the range of (a) 0~+1.1 V, (b) 0~+1.3 V, (c) 0~+1.5 V, (d) 0~+1.7 V and (e) 0~+1.9 V. Scan rate: 1 V s⁻¹.

S4 | Atomic force microscopy images of AM HOPG after the removal of droplet

AFM imaging of AM HOPG (in air) was performed to characterize the morphology of surfaces after treating the droplet (1 mM NaClO₄) resting on the surface with different methods, i.e. no voltage applied, constant potential (2 V) for 2 min, and 30 cyclic scans from 0 to +2 V (Figure S4). There was little change in the surface morphology from a freshly cleaved surface if the droplet was simply placed in contact with the surface (Figure S4a). With the potential held at 2 V, surface features appeared around step edges (Figure S4b). These features are also seen after potential cycling (Figure S4c), with further features across the basal surface, which have a density of 9 μm⁻², similar to the estimated point defect density on HOPG.^{1,2}

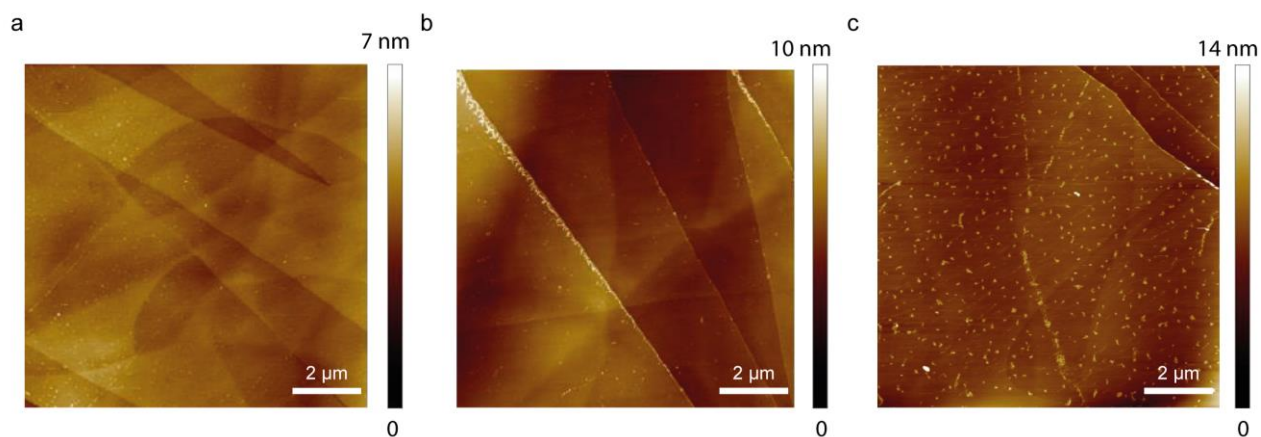


Figure S4. 10 μm × 10 μm AFM images of AM HOPG after removal of a droplet of 1 mM NaClO₄ solution that had resided on the surface (a) for 2 min without any voltage applied, (b) for 2 min with the voltage held at 2 V and (c) with the voltage swept from 0 to 2 V for 30 cycles (1 V s⁻¹).

S5 | X-ray photoelectron spectroscopy measurement of AM HOPG control sample

A droplet of 1 mM NaClO₄ solution was placed on the freshly-cleaved HOPG sample and left for the same time as on the electrochemically-treated sample (see main text and corresponding spectrum in Figure 6), before being blown away with an argon gas gun. XPS measurements were carried out on the surface immediately afterwards, with the spectrum showing only the presence of adsorbed ClO₄⁻ ions and residual NaClO₄ (Figure S5).

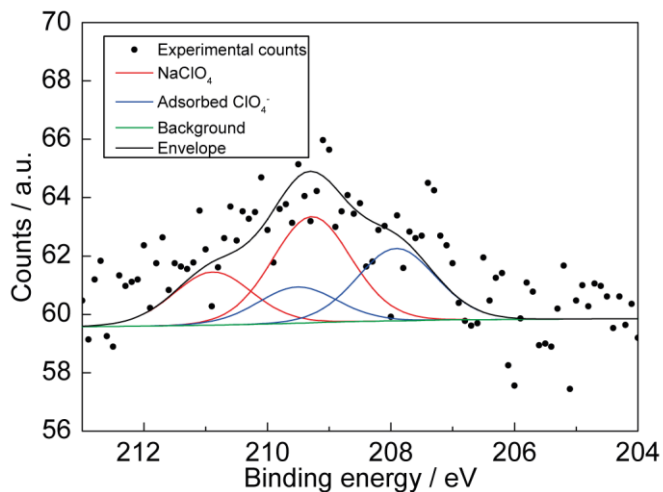


Figure S5. XPS spectrum of Cl 2p region on AM HOPG, without electrochemical treatment. The spectrum has been fitted with peaks for different species as indicated in the figure. The sum of fitting curves (black solid line) is consistent with the raw data (black dots).

S6 | Electrowetting of a droplet of 1 mM NaClO₄ solution on HOPG with the electric circuit on and off

Optical images in Figure S6 shows the electrowetting of a droplet of 1 mM NaClO₄ solution during CV carried out in the potential range of 0~+2 V (0.3 V s⁻¹). On the forward scan, at +1.68 V, the CE/RE disconnected with the droplet, due to significant electrowetting, and when the scan was finished at 0 V, a connection was made manually, leading to the recovery of the droplet from spreading.



Figure S6. Optical images of a droplet (1 mM NaClO₄) on AM HOPG during CV performed over the potential range of 0~+2 V, recorded at a potential of (a) 0 V (at the start of CV); (b) +1.68 V (on the forward scan), when the droplet detached from the CE/RE due to significant electrowetting and (c) 0 V (at the end of CV), when the electric circuit was re-connected. Scan rate: 0.3 V s⁻¹. The contact angle is marked in each image.

S7 | Potential polarity effect on the electrowetting of a droplet of 1 mM NaClO₄ solution on AM HOPG

CV measurements were also carried out from 0 to -2 V (1 V s^{-1}), in the droplet of 1 mM NaClO₄ solution on AM HOPG. As shown in Figure S7, no significant changes were seen in contact angle and relative contact diameter during the scan. This demonstrates that there is almost no electrowetting in the negative potential window.

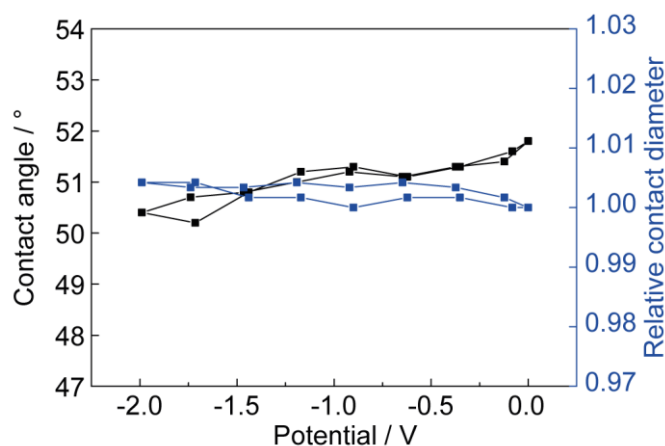


Figure S7. Contact angle and relative contact diameter of electrowetting for a droplet of 1 mM NaClO₄ solution at the surface of AM HOPG plotted against the potential of a CV carried out in the range of 0~-2 V, with a scan rate of 1 V s^{-1} .

S8 | Cyclic voltammograms of a droplet containing 1 mM Na₂SO₄, Na₃PO₄ or sodium fluorescein on AM HOPG

CV measurements were carried out from 0 V to +2 V at a scan rate of 1 V s⁻¹, with a droplet of 1 mM Na₂SO₄ solution (Figure S8). A reduction peak on the reverse sweep was seen at +0.4 V, similar to that observed for NaClO₄, which is attributed to anion de-intercalation.

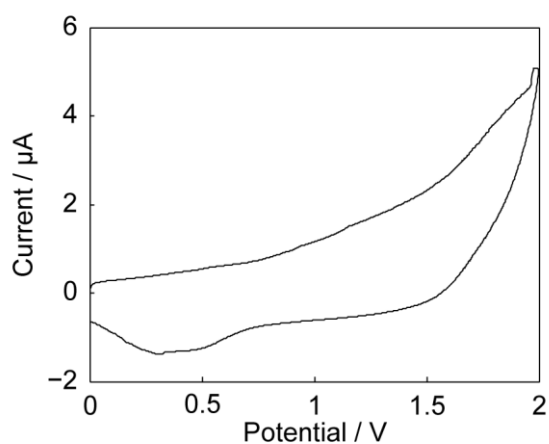


Figure S8. Cyclic voltammogram of a droplet of 1 mM Na₂SO₄ solution on AM HOPG, recorded from 0 V to +2 V at a scan rate of 1 V s⁻¹.

CVs for droplets containing 1 mM Na₃PO₄ (adjusted to pH ~7) or 1 mM sodium fluorescein on AM HOPG were also recorded (Figure S9). There were no obvious peaks for the intercalation/de-intercalation of ions over the potential range investigated.

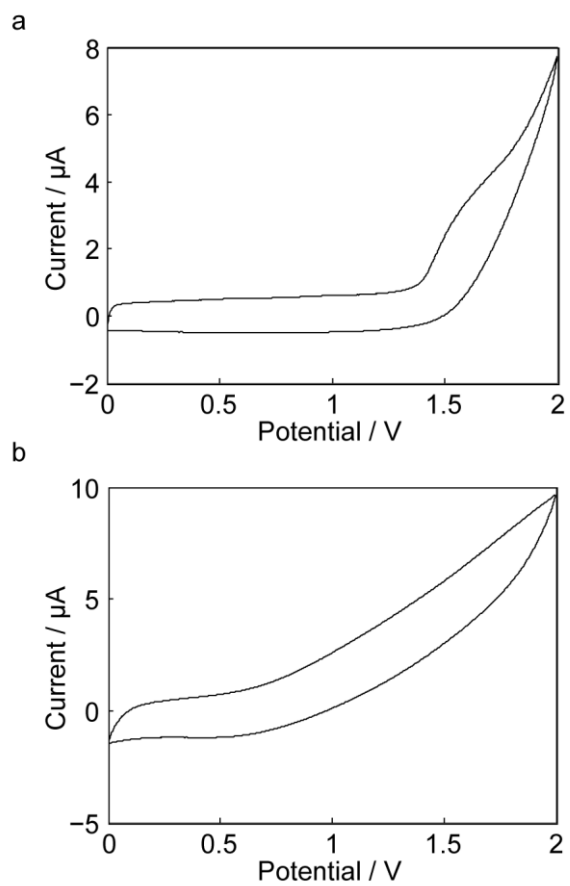


Figure S9. Cyclic voltammograms of a droplet of (a) 1 mM Na_3PO_4 solution (pH ~ 7) and (b) 1 mM sodium fluorescein solution on AM HOPG at a scan rate of 1 V s^{-1} .

References

1. Chang, H.; Bard, A. J. Scanning Tunneling Microscopy Studies of Carbon-Oxygen Reactions on Highly Oriented Pyrolytic Graphite. *J. Am. Chem. Soc.* **1991**, *113* (15), 5588-5596.
2. Chang, H.; Bard, A. J. Formation of Monolayer Pits of Controlled Nanometer Size on Highly Oriented Pyrolytic Graphite by Gasification Reactions as Studied by Scanning Tunneling Microscopy. *J. Am. Chem. Soc.* **1990**, *112* (11), 4598-4599.